

The [Y/Mg] chemical clock in the Galactic Disk [★]

The influence of metallicity and Galactic population in the solar neighbourhood

J. Shejeelammal, Jorge Meléndez, Anne Rathsam, and Giulia Martos

Universidade de São Paulo, Instituto de Astronomia, Geofísica e Ciências Atmosféricas, IAG, Departamento de Astronomia,
Rua do Matão 1226, Cidade Universitária, 05508-090, SP, Brazil
e-mail: shejee1a@usp.br, jorge.melendez@iag.usp.br

Received XXX; accepted YYY

ABSTRACT

Context. Stellar ages are an important parameter to study the chemical evolution of the Galaxy. To further the age estimates, various complementary methods to the conventional isochrone-fitting method have been implemented in the last decade. In recent years, several studies have established the existence of a relationship between chemical clocks and stellar ages. The [Y/Mg] clock is a promising technique, but there are still several open questions, such as its validity for metal-poor stars and differences between the thin and thick disk populations.

Aims. Our aim is to study the behaviour of the [Y/Mg] chemical clock with stellar ages for a sample of solar-type disk stars and to provide the empirical dating relation(s) for the stellar age determination from their precise chemical abundances. We also intend to study the effect of metallicity and population on this chemical clock.

Methods. We have derived the precise stellar atmospheric parameters as well as the elemental abundances of Mg and Y through line-by-line differential spectroscopic analysis for a sample of 48 metal-poor solar-type stars based on high-quality, high-resolution ESO/HARPS spectra. From the high-precision Gaia astrometric data, stellar masses and ages were estimated through isochrone-fitting using Yonsei-Yale isochrones. A joint analysis of our sample, together with a sample of 185 solar-twins and analogues from our previous works, is performed to calibrate the [Y/Mg] chemical clock in the Galactic disk for $-0.71 \leq [\text{Fe}/\text{H}] < +0.34$. Open clusters and stars with asteroseismic ages have been used to validate our relations.

Results. Two different populations could be clearly seen in the [Mg/Fe] - [Fe/H] plane - the thick and thin disks. Thick disk stars show an Age-Metallicity Relation (AMR), whereas the thin disk shows a flatter age-metallicity distribution. We found a strong anti-correlation between the [Y/Mg] ratio and the stellar ages of our sample, which is metallicity-dependent. For the first time in the literature, we report similar correlations for the thin and thick disk stars.

Conclusions. We find that the [Y/Mg] relation(s) found here for solar-type stars in a wide metallicity range is compatible with the literature using solar-twins. Our relation provides higher accuracy and precision of 0.45 and 0.99 Gyr, respectively, comparable with the best accuracy achieved for the solar-twins till date.

Key words. stars: abundances – Galaxy: disk – stars: solar-type – solar neighborhood – techniques: spectroscopic

1. Introduction

Besides the precise chemical abundances, the stellar age is an important parameter to study Galactic archaeology. Combining the accurate age estimates with the existing high-precision abundance data can pave the way to a better understanding of the Galactic chemical evolution (Bland-Hawthorn & Gerhard 2016; Alfredo Collazos 2023). To overcome the problems in the conventional isochrone fitting technique, several complementary methods have been investigated for the precise determination of stellar ages in the last decade (e.g. Soderblom 2010; Howes et al. 2019). Chemical clocks - abundance ratios that show a linear relationship with stellar ages - are important among these (e.g. Nissen 2015; Tucci Maia et al. 2016; Feltzing et al. 2017; Jofré et al. 2020).

da Silva et al. (2012) provided the first evidence of linear relation between abundance ratios and stellar ages. One of the most studied chemical clocks is the [Y/Mg] ratio, and it has been identified that it is a potential indicator of age in the case of solar-

twins (da Silva et al. 2012; Nissen 2015, 2016; Tucci Maia et al. 2016; Spina et al. 2016, 2018). Later, this relation was found to be valid for solar analogues (Nissen et al. 2017, 2020), solar-metallicity giants (Slumstrup et al. 2017), and red clump stars (Casamiquela et al. 2021) in the solar neighbourhood. Skúladóttir et al. (2019) explored the chemical clock outside the Galaxy and found that [Y/Mg] can be used as a chemical clock in dwarf galaxies.

Feltzing et al. (2017) identified for the first time the metallicity dependence of the [Y/Mg] clock and noted that it is valid only for $[\text{Fe}/\text{H}] > -0.5$. The metallicity dependence of the [Y/Mg] chemical clock has been later confirmed by Delgado Mena et al. (2018, 2019); Casali et al. (2020). Casali et al. (2020) first identified that the [Y/Mg] - Age relation is not universal and depends on the Galactocentric distance (R_{GC}), which was further investigated by Viscasillas Vázquez et al. (2022). It shows large dispersion outside the solar neighbourhood (Casali et al. 2020; Casamiquela et al. 2021).

The dependence of the chemical clocks on other parameters, such as stellar mass and temperature, has been explored by Delgado Mena et al. (2019). The validity of the [Y/Mg] clock for

[★] Based on data obtained from the ESO Science Archive Facility with DOI <https://doi.org/10.18727/archive/33>

thin and thick disk populations of the Galaxy has also been investigated in the literature and different correlations for these two components have been identified (Delgado Mena et al. 2018; Titarenko et al. 2019; Tautvaišienė et al. 2021). These studies have shown that the chemical clock is applicable only to thin disk stars.

The chemical dating can be closely related to the chemical evolution of the Galaxy and its different components (e.g. Haywood et al. 2013, 2016). The aim of this paper is to study the [Y/Mg] - Age relation in the solar neighbourhood of the Galactic disk over a wide metallicity range. Our analysis is based on a combined sample of 233 solar-type stars spanning the metallicity $-0.7 \leq [\text{Fe}/\text{H}] < +0.34$. We have examined the metallicity dependence of the [Y/Mg] chemical clock using this sample. There are not many studies in the literature exploring the trend of [Y/Mg] with stellar ages for the thick disk, and the findings are not always consistent. This has also been investigated in this study. This paper is structured as follows: Sect. 2 discusses the stellar sample and source of high-resolution spectroscopic data. In Sect. 3, we present the spectroscopic analysis. Results are discussed in Sect. 4. Finally, concluding remarks are presented in Sect. 5.

2. Stellar sample and spectroscopic data

Our analysis is based on a sample that contains three classes of stars of different similarity to the Sun - solar-twins, solar-analogues and solar-type (solar-like) stars. Solar-twins are the stars with parameters $\Delta T_{\text{eff}} = 100$ K, $\Delta \log g = 0.1$ dex, and $\Delta[\text{Fe}/\text{H}] = 0.1$ dex of the solar values (Meléndez et al. 2006; Ramírez et al. 2009). Solar-analogues are the dwarf stars with parameters $\Delta T_{\text{eff}} = 500$ K and $\Delta[\text{Fe}/\text{H}] = 0.3$ dex of the solar values (Soderblom & King 1998; Yana Galarza et al. 2016). Solar-type stars are those similar to the Sun in mass and evolutionary stage, belonging to the F8V to K2V spectral types with a B-V color in the range of 0.5 to 1.0 (Cayrel de Strobel 1996; Soderblom & King 1998).

The stellar sample consists of 48 solar-type Galactic disk stars selected from an updated catalogue of stellar parameters from Ramírez & Meléndez (2005), with parameters $5600 \text{ K} \leq T_{\text{eff}} \leq 6400 \text{ K}$, $4.1 \leq \log g \leq 4.6$, $-0.71 \leq [\text{Fe}/\text{H}] \leq -0.3$, and $0.85 \leq M \leq 1.05 M_{\odot}$. To have a wider metallicity range in the sample, in addition to these 48 metal-poor objects, we have included 185 solar-twins and analogues ($-0.3 \leq [\text{Fe}/\text{H}] < +0.34$) from our previous studies (Spina et al. 2018; Martos et al. 2023; Rathsam et al. 2023). Thus, our final sample consists of 233 solar-type¹ stars spanning the metallicity range $-0.71 \leq [\text{Fe}/\text{H}] < +0.34$.

For all the stars, the high-resolution spectra at $R \sim 115,000$ acquired using HARPS spectrograph were taken from the ESO (European Southern Observatory) archive (http://archive.eso.org/wdb/wdb/adp/phase3_spectral/form). These spectra cover the wavelength range 3780 - 6910 Å. Since we need high-quality spectra for a high-precision analysis, we have selected multiple spectra of the same objects with individual S/N in the range 30 - 370. In order to minimise the effect of telluric contamination on the spectral lines, we have used at least five spectra taken on different nights. Then the spectra were radial velocity corrected using IRAF (Image Reduction and Analysis Facility; <https://iraf-community.github.io/>), and then combined to get the final spectra. The final S/N of the combined spectra ranges from 360 to ~ 1000 . The combined spectra were

¹ Hereafter, we refer to the whole sample as solar-type stars because it contains all the three type stars

normalized by splitting them into seven segments, using IRAF. The continuum normalization of each individual segment was done iteratively using cubic spline polynomial of similar orders for the same segments, by evaluating the residuals as well as the visual fit to the continuum. Finally, the normalized segments are combined using IRAF. The spectra taken before and after the HARPS upgrade (June, 2015) were treated separately due to the difference in the shape of the continuum, and combined afterwards. In addition to the spectra of the stellar sample, we have also acquired HARPS solar spectra at the same resolution obtained from the asteroid Vesta.

3. Spectroscopic Analysis

The stellar atmospheric parameters as well as the elemental abundances were determined through a line-by-line differential analysis (Meléndez et al. 2012, 2014; Bedell et al. 2014) with respect to the Sun using the Python code *q²* (qoyllurquipu; <https://github.com/astroChasqui/q2>; Ramírez et al. 2014), adopting the line list from Meléndez et al. (2014). The equivalent width (EW) of each spectral line is measured on a star-by-star basis, including those in the Sun, performing deblending whenever necessary. For these calculations, *q²* uses the ATLAS9 Kurucz grid of model atmospheres (Castelli & Kurucz 2003) and the *ABFIND* driver of the code MOOG (version 2019; Sneden 1973; Sneden et al. 2012) that employs Local Thermodynamic Equilibrium (LTE).

3.1. Stellar atmospheric parameters

We have used the EW measurements of 91 Fe I and 18 Fe II lines to determine the atmospheric parameters. The final atmospheric parameters were determined in an iterative process from the initial guess of parameters using the differential excitation, ionization, and reduced EW (= EW/ λ) balances. The adopted solar atmospheric parameters are $T_{\text{eff}} = 5777$ K, $\log g = 4.44$ dex, $\zeta = 1 \text{ km s}^{-1}$, and $[\text{Fe}/\text{H}] = 0$ dex (Cox 2000). The code also evaluates the uncertainty on each atmospheric parameter following the procedures in Epstein et al. (2010) and Bensby et al. (2014), which is the cumulative uncertainty that includes the uncertainty on the measurements as well as the uncertainty that arises due to the mutual dependence of the atmospheric parameters. The typical precisions on the estimated atmospheric parameters of our sample are $\sigma(T_{\text{eff}}) = 10$ K, $\sigma(\log g) = 0.03$ dex, $\sigma(\zeta) = 0.02 \text{ km s}^{-1}$, and $\sigma([\text{Fe}/\text{H}]) = 0.007$ dex.

Following the determination of the stellar atmospheric parameters and their uncertainties, *q²* automatically uses the appropriate model atmospheres to calculate the chemical abundances using the MOOG code under LTE.

3.2. Chemical abundances: Mg and Y

The abundances of the elements Mg and Y are measured for each star using the same differential equivalent width method as the above. All the elemental abundances are scaled relatively to those obtained for the Sun on a line-by-line basis. We noted that, in all the metal-poor stars, the differential abundance derived from the Mg I 4730.040 Å line is lower by around ~ 0.05 dex compared to other Mg I lines. So, in order to get the consistent abundance values from all the Mg lines, we have applied an offset of -4 mÅ to the measured EW of this line in the Sun. The Mg I lines at 6318.717 and 6319.236 Å are contaminated by nearby telluric absorption features in a few stars, and in those

cases these lines were not considered in their abundance determination.

Yttrium shows hyperfine splitting (HFS), and is taken into consideration while calculating its abundances. It is employed by q^2 through the *blends* driver in the MOOG code and the adopted Y hyperfine lines from the Kurucz database.

The mean errors on the estimated abundances of Mg and Y are $\langle\sigma[\text{Mg}/\text{Fe}]\rangle = 0.01$ dex and $\langle\sigma[\text{Y}/\text{Fe}]\rangle = 0.02$ dex, respectively.

3.3. Stellar masses and ages

The masses and ages of the stellar sample were determined using the code q^2 , employing the spectroscopically determined atmospheric parameters and the Yonsei-Yale isochrones (Yi et al. 2001; Kim et al. 2002). Since our stars show non-solar abundances ($[\alpha/\text{Fe}] \neq 0$), the [Fe/H] values do not represent their actual metallicity. Hence, to account for the effect of α -enhancement on the global metallicity of the stars, we applied a correction factor $+\log_{10}(0.64 \times 10^{[\alpha/\text{Fe}]} + 0.36)$ (Salaris et al. 1993), together with an offset of -0.04 to recover the age and mass of a star with solar parameters, to the [Fe/H], as described in Spina et al. (2018). However, for the stars with [Fe/H] < 0, the effect of α -enhancement is already incorporated in the Yonsei-Yale isochrones to follow the Galactic trend, using the [α/Fe] values given in Meléndez et al. (2010). We have to subtract this factor to avoid double α -enhancement. For the stars in the metallicity range $-1 \leq [\text{Fe}/\text{H}] \leq 0$, the value is given by $[\alpha/\text{Fe}] = -0.3 \times [\text{Fe}/\text{H}]$. So, the final global metallicity ([M/H]) of the stars in our sample is given by Eq. 1, where we have used our estimates of [Mg/Fe] as a proxy for [α/Fe].

$$[\text{M}/\text{H}] = [\text{Fe}/\text{H}] - 0.04 + \log_{10}(0.64 \times 10^{[\text{Mg}/\text{Fe}]} + 0.36) - \log_{10}(0.64 \times 10^{-0.3 \times [\text{Fe}/\text{H}]} + 0.36) \quad (1)$$

The q^2 code produces a probability distribution for stellar masses and ages through an isochrone fitting, where the spectroscopic stellar parameters are compared with those obtained from the grid of isochrones (Ramírez et al. 2014). The most probable values of these probability distributions are adopted as stellar masses and ages, and the $1-\sigma$ range around the most probable values are taken as their respective uncertainties.

For this calculation, we have used the parallax values adopted from the Gaia DR3 (Gaia Collaboration et al. 2016, 2022; Babusiaux et al. 2022; <https://gea.esac.esa.int/archive/>), and the V magnitudes from the SIMBAD. If the V magnitudes were not available, then we estimated it using the Gaia G magnitudes and (BP - RP) colour-indices through the calibration equation given by Rathsam et al. (2023).

The ages and masses of the solar-twins from Spina et al. (2018) were recalculated using the same procedure as our sample, for consistency in the analysis, and are listed in Martos et al. (2023). The typical uncertainties in the isochrone ages and masses of the stellar sample are ~ 0.4 Gyr and $0.01 M_{\odot}$, respectively.

4. Results and discussion

Here, we discuss the results of our analysis of the combined sample of 233 disk stars (48 solar-type stars from this study and 185 solar-twins and analogues from our previous studies). The estimated stellar atmospheric parameters, masses, ages, and the

abundance ratios of our sample are given in Table A.1, and those of solar twins and analogues are given in Table A.2. The parameters of the combined sample are $5149 \text{ K} \leq T_{\text{eff}} \leq 6210 \text{ K}$, $4.04 \leq \log g \leq 4.57$, $-0.71 \leq [\text{Fe}/\text{H}] < 0.34$, and $0.82 \leq M \leq 1.1 M_{\odot}$, and all the stars lie in the solar neighbourhood ($R_{GC} \sim 8$ kpc).

4.1. Bi-modality of the Galactic disk and Age-Metallicity-Relation (AMR)

Figure 1 shows the [Mg/Fe] ratio with respect to the [Fe/H] of the combined sample. From this figure, we can clearly see two populations of [Mg/Fe] at low-metallicity, the high- α or thick disk and the low- α or thin disk. At higher metallicities ($[\text{Fe}/\text{H}] \geq 0$), both populations are indistinguishable. This bimodality of the Galactic disk in the $[\alpha/\text{Fe}] - [\text{Fe}/\text{H}]$ plane has already been identified in several previous studies (e.g. Reddy et al. 2006; Adibekyan et al. 2011, 2012; Haywood et al. 2013; Nidever et al. 2014; Bensby et al. 2014; Ness et al. 2019; Weinberg et al. 2019; Xiang & Rix 2022; Leung et al. 2023; Imig et al. 2023; Patil et al. 2023). It is the consequence of different chemo-dynamical evolution and star formation history of the Milky Way disk (e.g. Haywood et al. 2013; Bergemann et al. 2014; Casagrande et al. 2011). Generally, thick disk is composed of old, metal-poor, α -enhanced stars, whereas thin disk is composed of younger, α -poor stars (Fuhrmann 1998; Bensby et al. 2005; Lee et al. 2011). However, there is no obvious method to completely disentangle these two components of the Galactic disk and to identify purely thin/thick disk stars in the solar neighbourhood (Bensby et al. 2003; Adibekyan et al. 2012; Haywood et al. 2013). Furthermore, the separation between the α -sequences and even the existence of boundary between these two populations (Bovy et al. 2012a) are still topics of debate. A detailed review on Galactic disk can be found in Rix & Bovy (2013).

Previously, the thin/thick disk stars were distinguished either from a pure kinematical approach (e.g. Bensby et al. 2003; Reddy et al. 2006) or from an approach combining kinematics, metallicity, and age (e.g. Haywood 2008). However, both these methods are found to be prone to ‘contamination’ or overlap between the two components (Bensby et al. 2003; Adibekyan et al. 2012; Bovy et al. 2012b). In addition to this, the radial migration is proposed to have redistributed the stars in the solar neighbourhood (e.g. Liu & van de Ven 2012; Haywood et al. 2013). This radial migration and the higher eccentric orbits lead to the contamination of the kinematically selected thin/thick disk stars in the solar vicinity (e.g. Schönrich & Binney 2009).

The advent of several large sky multi-object spectroscopic surveys in the last decade allowed the chemo-kinematic analysis of much larger samples of stars. As a consequence, a purely chemical approach to dissect the Galactic disk began to gain significance. Several studies have shown that chemical dissection of the Galactic disk is more reliable because the chemical composition of a star is a more stable property that is closely related to the time and place of birth, whereas the kinematics and spatial positions change all the time (Navarro et al. 2011; Adibekyan et al. 2011; Liu & van de Ven 2012; Bovy et al. 2012b; Adibekyan et al. 2012, 2013). It has also been proposed that various properties (scale height, kinematics etc.) of different Galactic stellar populations can be parametrized using their chemical composition (Bovy et al. 2012b).

For a given age, the solar vicinity exhibits a broader metallicity distribution since stars of different birth radii (and hence different metallicities) contribute to the local neighbourhood (Liu & van de Ven 2012). As a result, despite the fact that the thick disk is comparatively older, stars with a range of ages and metal-

licities can contribute to both thin and thick disks, giving rise to a large overlap in metallicity. Hence, even though the chemical composition is the more reliable approach, the metallicity ($[\text{Fe}/\text{H}]$) alone is not an ideal choice. From the chemo-orbital analysis of a sample of SDSS/SEGUE (Yanny et al. 2009) data, Liu & van de Ven (2012) have shown that the α -abundance is preferred because it is relatively independent of birth radii and is a more appropriate proxy for age. The distribution of $[\alpha/\text{Fe}] - [\text{Fe}/\text{H}]$ ratio has been used in several studies to distinguish between the two disk populations (e.g. Adibekyan et al. 2011; Haywood et al. 2013). The limit characterizing the thin/thick disk populations is defined empirically, by examining the chemical separation in $[\alpha/\text{Fe}]$ between the high- α (thick disk) and low- α (thin disk) sequences. Recent studies based on the chemo-kinematical and statistical methods using large samples from high-resolution spectroscopic surveys like APOGEE (e.g. Anders et al. 2014; Patil et al. 2023), Gaia - ESO Survey (e.g. Gent et al. 2024), GALAH (e.g. Cantelli & Teixeira 2024) etc. have shown that the decomposition of the Galactic disk is better understood in terms of the chemical enrichment (α abundance).

On the ground of the above discussion, we have adopted the chemical separation given in Adibekyan et al. (2011) to separate the thin and thick disk sequences. This is shown as a red solid line in the $[\text{Mg}/\text{Fe}] - [\text{Fe}/\text{H}]$ plane in Fig. 1. We identified the stars above this line as thick disk stars and those below as thin disk stars². The behaviour of $[\text{Mg}/\text{Fe}]$ ratio with respect to various orbital properties and the Toomre diagram of our sample are shown in Figs. B.1 and B.2. As seen in the several previously mentioned works, our chemically defined thick and thin disk stars are mixed in the kinematic plane. The thick disk contains the older stars (age > 8 Gyr; two stars have ages 6.7 and 7.5 Gyr) of the sample, whereas the thin disk shows an age spread. All the youngest stars of the sample belong to the thin disk.

We note that a younger star with an age of 4.6 Gyr is a member of the thick disk (cyan circle; Fig. 1 lower panel). This object, HD 65907, show anomalous behaviour compared to other stars of the sample. As could be seen from the figures, it lies well off the other objects of its kind. Fuhrmann et al. (2012) analysed this anomalous object, and from its chemical abundance they identified it as an old, population II, thick disk star with an age of 12 or 13 Gyr. However, the age inferred from the evolutionary tracks is $5.6^{+2.2}_{-1.8}$ Gyr, which contradicts its chemical properties. According to Fuhrmann et al. (2012), this discrepancy could be resolved only with a mass accretion scenario on HD 65907. So, this object is probably a product of former mass-transfer event, like the solar analogue HIP 10725 (Schirbel et al. 2015).

The Age-Metallicity Distribution (AMD) of the whole sample is shown in Fig. 2. From earlier studies, it has been identified that the age and metallicity are not strongly correlated in the solar neighbourhood, and the metallicity shows a significant scatter for the same age (e.g. Edvardsson et al. 1993; Feltzing et al. 2001; Haywood 2006; Casagrande et al. 2011; Bensby et al. 2014; Lin et al. 2020; Sahlholdt et al. 2022; Patil et al. 2023). From Fig. 2, it is clear that stars of similar age show a large range of metallicities. The thick disk stars in the sample show an Age-Metallicity-Relation (Fig. 2, upper panel), as previously noted by Schuster et al. (2006); Bensby et al. (2014); Patil et al. (2023), and others. Meanwhile, the age and metallicity are uncorrelated for the thin disk stars, and show an almost flat distribution. However, both the populations are indistinguishable from each other in the Age - $[\text{Fe}/\text{H}]$ space.

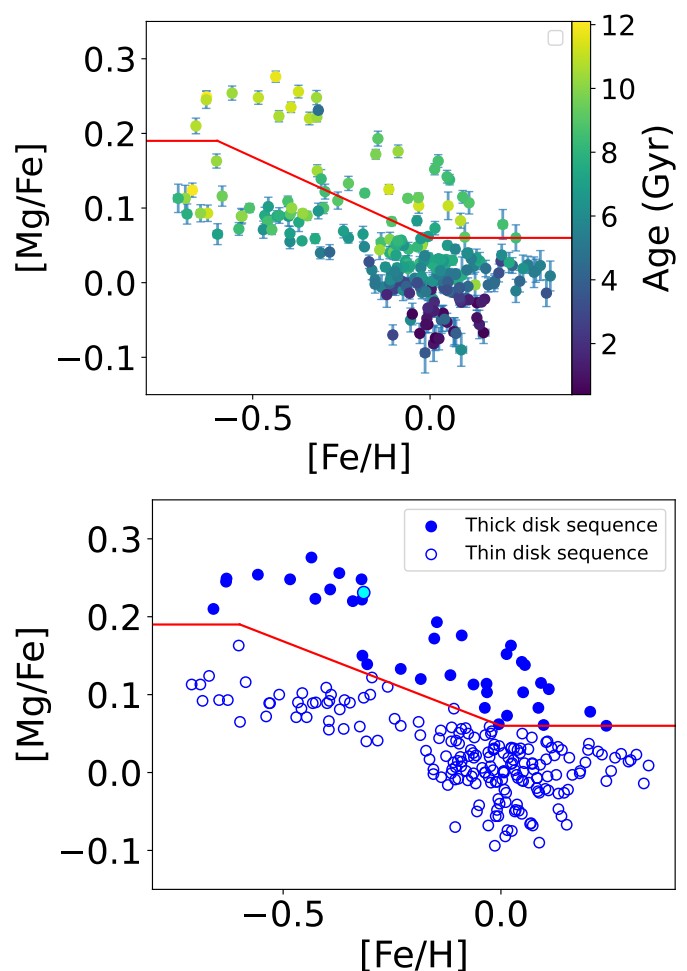


Fig. 1: $[\text{Mg}/\text{Fe}]$ ratio as a function of $[\text{Fe}/\text{H}]$ for the combined sample. The red solid line shows the separation between thin and thick disk stars based on the $[\text{Mg}/\text{Fe}]$ ratio similar to Adibekyan et al. (2011); $[\text{Mg}/\text{Fe}] = +0.19$ for $[\text{Fe}/\text{H}] \leq -0.6$, $[\text{Mg}/\text{Fe}] = -0.217 \times [\text{Fe}/\text{H}] + 0.06$ for $-0.6 < [\text{Fe}/\text{H}] \leq 0$, $[\text{Mg}/\text{Fe}] = +0.06$ for $[\text{Fe}/\text{H}] > 0$. Stars above this line belong to the Galactic thick disk. The cyan circle is the anomalous star HD 65907.

From the contour plot for the AMD of the stellar sample (bottom panel, Fig. 2), we note the following: (i) up to the age of ~ 12 Gyr and for $[\text{Fe}/\text{H}] > -0.2$, we see a flat AMR with a scatter in the metallicity (ii) for the older (age > 7 Gyr), metal-poorer stars in the sample ($[\text{Fe}/\text{H}] < -0.2$), we see a downward trend in the AMD (iii) the majority of the distribution is centred at $[\text{Fe}/\text{H}] \sim 0$ with a peak around ages between 4 - 9 Gyr. This is on par with the findings in the previous studies of the Galactic disk (e.g. Edvardsson et al. 1993; Feltzing et al. 2001; Bergemann et al. 2014). The AMR and the evolution of the Galactic disk are broader topics, and their detailed discussion is beyond the scope of this paper. There are several studies dedicated to the AMR in the Galactic disk using quite larger samples, to name a few, Feltzing et al. (2001); Lin et al. (2020); Sahlholdt et al. (2022); Patil et al. (2023).

4.2. Abundance trend with age

The distributions of $[\text{Mg}/\text{Fe}]$, $[\text{Y}/\text{Fe}]$, and $[\text{Y}/\text{Mg}]$ with respect to stellar ages of the combined sample are shown in Fig. 3. As

² Chemically defined

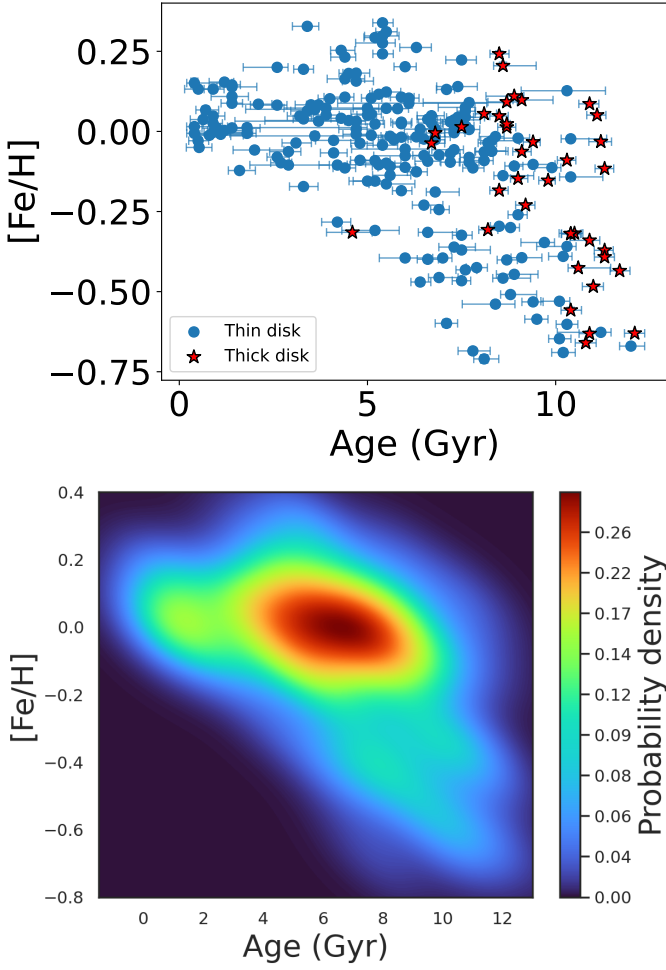


Fig. 2: Age-Metallicity Distribution of the sample. The red star that is off the other thick disk objects in the upper panel is the anomalous star HD 65907. The bottom panel is the density plot for the AMD of the sample.

could be seen from the [Mg/Fe] - [Fe/H] distribution (Fig. 1), the thin and thick disk objects show a clear dichotomy in the [Mg/Fe] - Age plane as well. The [Mg/Fe] and [Y/Fe] ratios show positive and negative slopes, respectively, with respect to age, as expected from their origin and chemical evolution models. Mg is an α -element produced by Type II Supernovae (SNe II) on a shorter time scale ($\leq 10^7$ yrs; e.g. Kobayashi et al. 2006). SNe II were the main contributors of metals to the Interstellar Medium (ISM) during the early stages of the chemical evolution. So, α -elements show a positive trend with respect to age. Y is an s-process element produced in low- and intermediate-mass Asymptotic Giant Branch (AGB) stars, which contributed to the chemical evolution much later compared to SNe II. As a result, Y shows a negative trend with stellar ages (Nomoto et al. 2013; Matteucci 2014; Karakas & Lattanzio 2014; Spina et al. 2016 and references therein).

As a consequence of different origins and chemical evolution, the [Y/Mg] ratio has a steeper dependence on stellar ages. As seen from Fig. 3 (bottom panel), the [Y/Mg] ratio of our sample shows a strong anti-correlation with age. The scatter in the [Y/Mg] ratio of our sample is small compared to that found in other samples of solar-type stars in the literature (e.g. Feltzing et al. 2017; Titarenko et al. 2019; Casali et al. 2020). We note continuity in the [Y/Mg] - Age correlation between the thin and

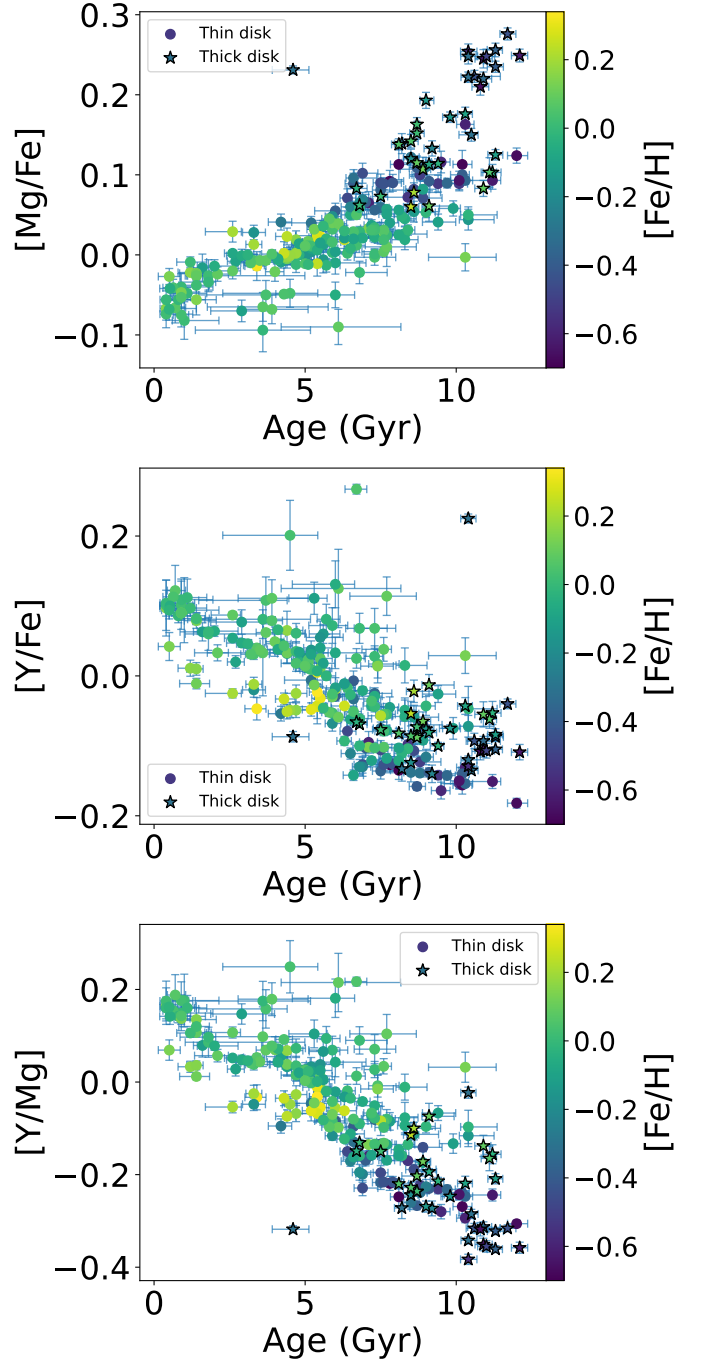


Fig. 3: [Mg/Fe], [Y/Fe], and [Y/Mg] ratios as a function of age for the combined sample, colour-coded by [Fe/H]. The star at ~ 5 Gyr is HD 65907, probably a result of a former mass-transfer event.

thick disk stars. We also note that there is no significant gradient of [Y/Mg] with respect to [Fe/H], as was seen in Feltzing et al. (2017).

4.3. The [Y/Mg] chemical clock

In this section, we analyse the [Y/Mg] - Age correlation in our sample. The stellar ages derived from the isochrone fitting have been used in this analysis. We have performed a simple linear regression fitting to derive the empirical relation connecting the

[Y/Mg] ratio and stellar ages, of the form $[Y/Mg] = a \times \text{Age} + b$. From the linear fitting, we found that the [Y/Mg] of the sample is correlated to the stellar age through the relation (Fig. 4):

$$[Y/Mg] = -0.040(\pm 0.001) \times \text{Age (Gyr)} + 0.186(\pm 0.036) \quad (2)$$

In order to get the best possible relation, we have eliminated a few stars that lie outside the bulk of the sample in the [Y/Mg] - Age space. The outlier limit is set at the 2σ level of the trend (Eq. 2), which is given by the linear function $[Y/Mg] = -0.040 \times \text{Age (Gyr)} + 0.356$, as shown in Fig. 4. We have also excluded the anomalous star HD 65907 from this analysis. We did not make any distinction between the thin and thick disk objects. From the linear fit shown in Fig. 5 for the sample after excluding the outliers, we obtained a relation of the form:

$$[Y/Mg] = -0.041(\pm 0.001) \times \text{Age (Gyr)} + 0.187(\pm 0.040) \quad (3)$$

However, from the analysis of a sample of 714 solar-type stars, Feltzing et al. (2017) first identified the metallicity dependence of the [Y/Mg] chemical clock, which was subsequently found in the samples of Delgado Mena et al. (2019) and Casali et al. (2020). In order to check the metallicity dependence of Eq. 3, we have examined the distribution of [Y/Mg] residuals ($\Delta[Y/Mg] = [Y/Mg]_{\text{obs}} - [Y/Mg]_{\text{pred}}$) with respect to metallicity to see if there exist any trend. As we can see from Fig. 6, the $\Delta[Y/Mg]$ is independent of metallicity up to a value of $[\text{Fe}/\text{H}] \sim -0.17$ and show a trend below that. This confirms that the [Y/Mg] chemical clock depends on the metallicity and the whole sample could not be represented using a single relation given in Eq. 3. Hence, we divided the sample into two metallicity bins, $-0.71 \leq [\text{Fe}/\text{H}] < -0.17$ and $-0.17 \leq [\text{Fe}/\text{H}] < +0.34$, and performed the fitting separately, as shown in Fig. 7. This simple linear fitting resulted in the following relations:

$$[Y/Mg] = -0.0362(\pm 0.0004) \times \text{Age (Gyr)} + 0.0867(\pm 0.0285);$$

(for $-0.71 \leq [\text{Fe}/\text{H}] < -0.17$)

$$[Y/Mg] = -0.0340(\pm 0.0006) \times \text{Age (Gyr)} + 0.1656(\pm 0.0346);$$

(for $-0.17 \leq [\text{Fe}/\text{H}] < +0.34$)

(4)

We have performed this fitting for five different metallicity bins of width 0.2 dex as well, and note that the results do not produce significant deviations from the results obtained using Eq. 4.

We then inverted the relations in Eq. 4 to get the stellar dating relations of the form:

$$\text{Age (Gyr)} = -27.6243(\pm 0.3053) \times [Y/Mg] + 2.3950(\pm 0.8139);$$

(for $-0.71 \leq [\text{Fe}/\text{H}] < -0.17$)

$$\text{Age (Gyr)} = -29.4118(\pm 0.5191) \times [Y/Mg] + 4.8706(\pm 1.1039);$$

(for $-0.17 \leq [\text{Fe}/\text{H}] < +0.34$)

(5)

Since we identified the metallicity dependence of the [Y/Mg] ratio in the sample, we have also performed a multivariate linear regression fitting by incorporating the $[\text{Fe}/\text{H}]$ as well. The obtained relation as a function of stellar age and metallicity is given by:

$$[Y/Mg] = -0.036(\pm 0.001) \times \text{Age (Gyr)} + 0.125(\pm 0.010) \times [\text{Fe}/\text{H}] + 0.165(\pm 0.034) \quad (6)$$

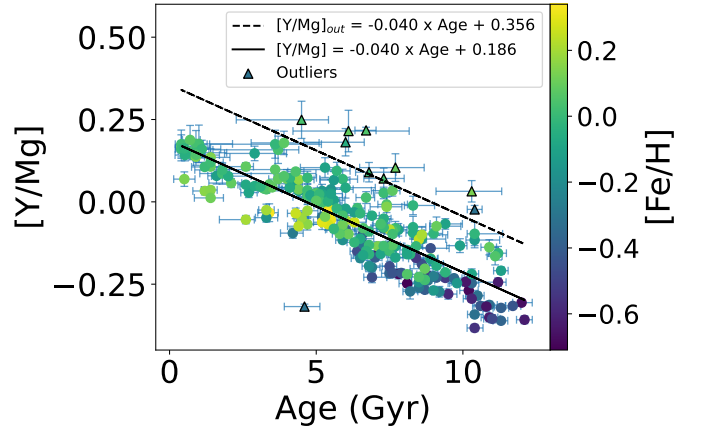


Fig. 4: Linear fit to the [Y/Mg] - Age distribution of the whole sample (black solid line) and the outlier cut (black dashed line). The outlier limit is set at the 2σ level of the trend. The triangle at the lower part of the plot is the anomalous star HD 65907.

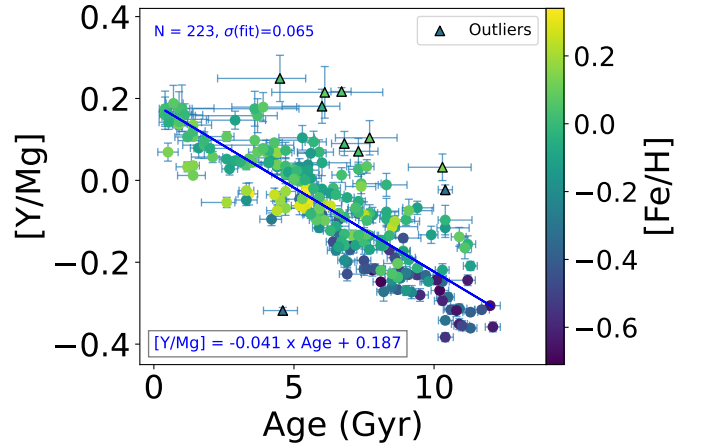


Fig. 5: Best linear fit (blue solid line) for the [Y/Mg] - Age distribution of the sample. The fitting function is described in the text.

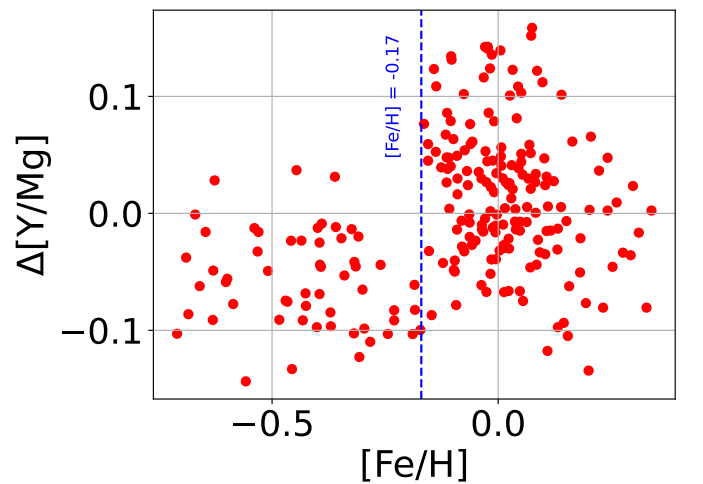


Fig. 6: Distribution of [Y/Mg] residuals ($\Delta[Y/Mg]$) with respect to metallicity of the sample. The vertical dashed line at $[\text{Fe}/\text{H}] = -0.17$ represents the point below which $\Delta[Y/Mg]$ shows an offset with metallicity.

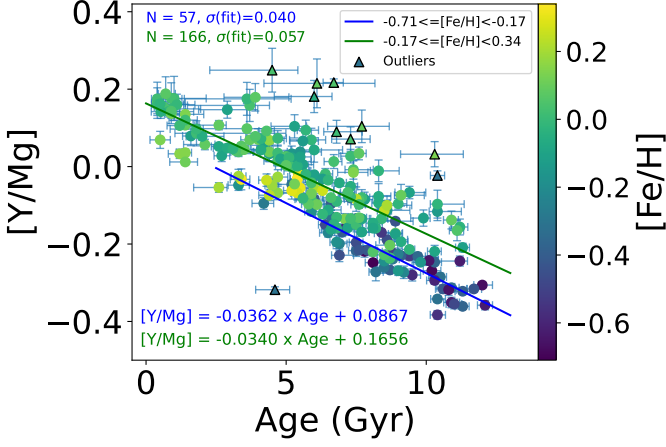


Fig. 7: [Y/Mg] - Age linear fits for the sample in two metallicity bins $-0.71 \leq [\text{Fe}/\text{H}] < -0.17$ (blue solid line) and $-0.17 \leq [\text{Fe}/\text{H}] < +0.34$ (green solid line).

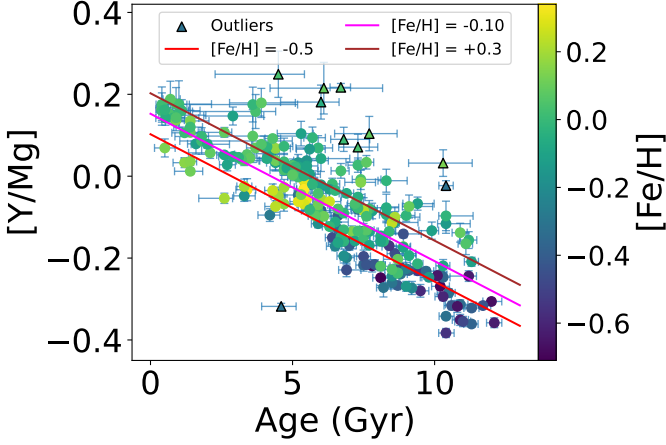


Fig. 8: Multivariate linear fits for the [Y/Mg] - Age distribution of the sample for three different metallicities. The fitting function is described in the text.

The chemical age is given by the relation:

$$\text{Age (Gyr)} = -27.701(\pm 0.461) \times [\text{Y}/\text{Mg}] + 3.454(\pm 0.329) \times [\text{Fe}/\text{H}] + 4.576(\pm 1.013) \quad (7)$$

Figure 8 shows the relation in Eq. 6 for three different metallicity values, $[\text{Fe}/\text{H}] = -0.5, -0.1$ and $+0.3$.

The chemical ages of the sample are calculated using both Eq. 5 and Eq. 7 and compared with the isochrone ages and with each other. The chemical ages do not show any trend with the isochrone ages (offset ~ 0). The standard deviation (S.D) of the single variate chemical age (Eq. 5, SV chemical age hereafter) with respect to the isochrone age is 1.55 Gyr and that of the multivariate chemical age (Eq. 7, MV chemical age hereafter) is 1.66 Gyr. We note that the average uncertainty in the isochrone ages of the sample is ~ 0.4 Gyr. As could be seen from the comparison between SV and MV chemical ages shown in Fig. 9, both ages match quite well with an offset of -0.005 Gyr. The mean scatter and SD between them are 0.50 and 0.62 Gyr respectively.

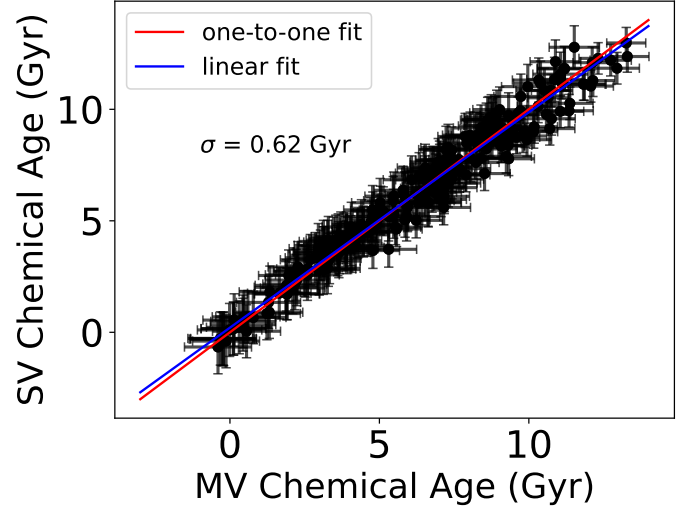


Fig. 9: Correlation between single variate (SV; Eq. 5) and multivariate (MV; Eq. 7) chemical ages of the stellar sample.

4.3.1. Validation using open clusters and stars with asteroseismic ages

In order to validate our relations in Eqs. 5 and 7, we have used the data for open clusters (OCs) and stars with asteroseismic ages. OCs are one of the powerful tools to validate the chemical clocks because the member stars of each cluster show homogeneity in age and chemical composition. As a result, their ages have been precisely determined through isochrone-fitting from the observation of several member stars (e.g. Casali et al. 2019; Viscasillas Vázquez et al. 2022). Casali et al. (2020) have presented a list of OCs selected from the iDR5 of the Gaia-ESO Survey (GES; Gilmore et al. 2012; Randich et al. 2013), with cluster membership probability of at least 80%. From this list, we have selected 13 OCs with $R_{GC} \geq 6.5$ kpc.

In the case of single stars, asteroseismology provides the reliable ages from the solar-like oscillations on the stellar surface (Chaplin & Miglio 2013; Silva Aguirre et al. 2012; Christensen-Dalsgaard 2016). Silva Aguirre et al. (2017) have presented the asteroseismic ages for a sample of 66 main-sequence stars (*Kepler* LEGACY sample; KLS hereafter) based on the asteroseismic data from the *Kepler* mission. The KLS is claimed to have the best asteroseismic data available among the solar-like stars. We have selected 10 stars from the KLS for which the precise abundances are available in the literature. The validation sample of OCs and KLS stars used to calibrate our chemical clocks are given in Table 1. The Y and Mg abundances of OCs and KLS stars are adopted from Casali et al. (2020) and Nissen et al. (2017), respectively.

Figure 10 shows the comparisons of the SV (upper panel) and MV (middle panel) chemical ages of the validation sample calculated using our relations with their literature ages. The lower panel of this figure shows the correlation between the SV and MV chemical ages of this sample. As can be seen from the figure, the OCs show a larger scatter compared to the KLS stars, but both agree with the [Y/Mg] clock within 1 or 2- σ . This may be because these cluster members are giant/sub-giants, whereas our relations are derived based on a sample of dwarf stars. In addition to this, even though the OCs lying in the inner Galactic disk ($R_{GC} < 6.5$ kpc) are excluded from our comparison, there could be a possibility that some of them originally belonged to this region and are currently in the solar-neighborhood as a result

of radial migration (e.g. [Viscasillas Vázquez et al. 2022](#)). Since our stellar sample lies in the solar neighbourhood, this also may have contributed to the scatter seen in Fig. 10.

Single variate chemical clock (Eq. 5): In the case of KLS stars with asteroseismic ages, the mean scatter (accuracy) of this chemical clock is 0.91 Gyr, with a standard deviation (S.D; precision) of 0.96 Gyr and a mean relative error (MRE)³ of 38%. The average uncertainty in the seismic ages of the sample is ~ 0.52 Gyr, and the [Y/Mg] has a mean error of 0.013 dex, which translates to ~ 0.32 Gyr. By incorporating these two errors in to the mean scatter, the actual accuracy of the SV chemical age is estimated to be ~ 0.67 Gyr for the KLS stars. In the case of OCs, the mean scatter and the S.D of the SV chemical clock are 1.10 and 1.24 Gyr, respectively. The average uncertainty in their isochrone ages is 0.23 Gyr and that from the [Y/Mg] ratio is 0.73 Gyr ($\equiv 0.03$ dex). Subtracting these errors results in an accuracy of 0.79 Gyr in the SV chemical ages of the OCs.

Multivariate chemical clock (Eq. 7): The mean scatter and the S.D are 0.76 Gyr and 0.99 Gyr, respectively, with a MRE of 33% for the KLS stars. In the case of OCs, the mean scatter and the S.D for this chemical clock are 1.17 Gyr and 1.45 Gyr, respectively. Incorporating the uncertainties in the literature ages and the [Y/Mg] ratios, the accuracy of the MV chemical ages is estimated to be 0.45 Gyr and 0.88 Gyr, respectively, for the KLS stars and the OCs.

In summary, the accuracy we have obtained using our chemical clocks based on the KLS stars with asteroseismic ages and the OCs with isochrone ages respectively are ~ 0.67 and 0.79 Gyr (SV chemical age) and ~ 0.45 and 0.88 Gyr (MV chemical age). These values are similar to the accuracy achieved for the solar-twin stars in the solar neighbourhood ($\sim 0.8 - 1$ Gyr; [Nissen 2015, 2016](#); [Tucci Maia et al. 2016](#); [Spina et al. 2018](#)). Since the KLS stars are dwarfs and lie in the close vicinity of the Sun as our stellar sample, the validation using them is likely more accurate compared to the OCs.

4.3.2. Chemical clock in the thin and thick disks

While the studies using solar-twins, analogues, and solar-type stars with $[\text{Fe}/\text{H}] \geq -0.3$ confirmed the tight correlation between the [Y/Mg] ratio and stellar ages irrespective of the population (thin/thick disk; [Nissen 2016](#); [Tucci Maia et al. 2016](#); [Spina et al. 2016, 2018](#); [Nissen et al. 2017, 2020](#); [Jofré et al. 2020](#)), a few recent studies have suggested that the [Y/Mg] chemical clock could only be used for thin disk stars, and may not be valid for lower metallicities or thick disk stars (e.g. [Feltzing et al. 2017](#); [Delgado Mena et al. 2018, 2019](#); [Titarenko et al. 2019](#); [Tautvaišienė et al. 2021](#)). [Feltzing et al. \(2017\)](#) have suggested that the [Y/Mg] - age distribution is almost flat and has no predictive power on age for $[\text{Fe}/\text{H}] < -0.5$. However, [Delgado Mena et al. \(2018\)](#) have shown that it still has a correlation with age (up to $[\text{Fe}/\text{H}] \sim -0.8$), but only for thin disk stars. The trend becomes flat for thick disk stars, and for thin disk stars with ages ≥ 8 Gyr. From an AMBRE sample of solar-type stars, [Titarenko et al. \(2019\)](#) identified different slopes for thin disk and thick disk stars with the thick disk stars showing a steeper dependence. Recently, [Tautvaišienė et al. \(2021\)](#) found that thick disk stars (233 stars including dwarfs and giants) show no trend of [Y/Mg] with age (slope ~ -0.002), contrarily to the slopes identified for the thick disk stars of [Titarenko et al. \(2019\)](#) and [Bensby et al. \(2014\)](#). This may be due to the different luminosity classes in their sample.

We have examined the dependence of the [Y/Mg] chemical clock on stellar age for the thin and thick disk stars separately and found that both components show almost the same correlation, with slopes $-0.039(\pm 0.001)$ and $-0.034(\pm 0.001)$, respectively. The linear fits (Eq. 8) for the two populations are shown in Fig. 11.

$$\begin{aligned} [\text{Y}/\text{Mg}]_{\text{Thin}} &= -0.039(\pm 0.001) \times \text{Age (Gyr)} + 0.178(\pm 0.038) \\ [\text{Y}/\text{Mg}]_{\text{Thick}} &= -0.034(\pm 0.001) \times \text{Age (Gyr)} + 0.089(\pm 0.015) \end{aligned} \quad (8)$$

Our results disagree with previous studies, which found that either the thick disk stars showed no trend at all or a different trend than the thin disk stars. In particular, the thick disk stars in [Spina et al. \(2018\)](#) seem to have a small offset relative to the [Y/Mg] - age relation defined by their thin disk sample. However, their sample of thick disk stars is relatively small, making it difficult to perform a separate fit for the [Y/Mg] - age relation of the thick disk. Although our sample size of thick disk stars has increased relative to the study of [Spina et al. \(2018\)](#), we have to keep in mind that our number is still relatively small (36 objects without outliers). We note that the results may be somewhat biased due to the selection biases of thick and thin disk stars in different studies.

4.3.3. Comparison with the previous works

The slopes of the [Y/Mg] - Age distribution for solar-twins and solar-type stars from different studies, along with our estimates, are given in Table 2. These estimates are based on the linear relation between [Y/Mg] and the stellar ages. We note that, while the relations obtained for the solar-twins by different authors are similar irrespective of the sample size, the solar-type stars give different slopes. However, [Nissen et al. \(2017\)](#); [Delgado Mena et al. \(2019\)](#); [Nissen et al. \(2020\)](#); [Tautvaišienė et al. \(2021\)](#) show similar values that match those of solar-twins. The lowest metallicity of these samples is -0.6 , and other studies of solar-type stars have comparatively wider range of metallicities. Hence, the difference in the slopes plausibly results from the metallicity dependence, as discussed in [Feltzing et al. \(2017\)](#); [Delgado Mena et al. \(2018, 2019\)](#). However, when we consider the sample irrespective of the population, our relations are compatible with those found for the solar-twins by [Nissen \(2016\)](#) and for solar-type stars by [Nissen et al. \(2017\)](#) and [Nissen et al. \(2020\)](#). While our estimate for the thick disk stars matches the estimate of [Tautvaišienė et al. \(2021\)](#) from a sample of 76 thick disk giants, it disagrees with other samples of thick disk stars. In the case of thin disk stars, our estimate is comparable with the value obtained by [Delgado Mena et al. \(2019\)](#).

The values listed in Table 2 are based on a simple linear regression fit between the chemical clock and the stellar ages. In light of the results from [Feltzing et al. \(2017\)](#); [Delgado Mena et al. \(2018\)](#), and the non-universality of the chemical clock - age relation in the Galactic disk ([Casali et al. 2020](#)), a few recent studies have attempted to perform multiple variable linear regression fitting by including the stellar atmospheric parameters, Galactocentric distances, stellar masses, etc. in addition to the stellar ages ([Delgado Mena et al. 2019](#); [Casali et al. 2020](#); [Viscasillas Vázquez et al. 2022](#)).

The accuracy and precision of the [Y/Mg] chemical clock when considered as function of age, $[\text{Fe}/\text{H}]$, and R_{GC} are 1.6 Gyr and 2.8 Gyr, respectively ([Viscasillas Vázquez et al. 2022](#)).

³ RE = $\frac{|\text{Literature age} - \text{Chemical age}|}{\text{Literature age}}$

Table 1: Properties of the OCs and KLS stars used in this study.

ID	[Fe/H] (dex)	[Y/Mg] (dex)	Age (Gyr)	ID	[Fe/H] (dex)	[Y/Mg] (dex)	Age (Gyr)
OCs*				KLS stars†			
Berkeley 31	-0.270±0.060	-0.010±0.030	2.50±0.30	KIC 3427720	-0.024±0.017	-0.017±0.015	2.40±0.30
Berkeley 36	-0.160±0.100	-0.050±0.060	7.00±0.50	KIC 6106415	-0.037±0.012	0.002±0.011	4.80±0.60
Berkeley 44	0.270±0.060	0.140±0.070	1.60±0.30	KIC 6225718	-0.110±0.014	0.051±0.012	2.60±0.40
M 67	-0.010±0.040	0.000±0.010	4.30±0.50	KIC 7940546	-0.126±0.012	0.056±0.010	2.40±0.30
Melotte 71	-0.090±0.030	0.070±0.010	0.83±0.18	KIC 9139151	0.096±0.019	0.101±0.017	1.90±0.70
NGC 2243	-0.380±0.040	-0.040±0.030	4.00±1.20	KIC 10162436	-0.073±0.021	0.071±0.017	2.50±0.40
NGC 2420	-0.130±0.040	0.070±0.030	2.20±0.30	KIC 10644253	0.130±0.019	0.066±0.017	1.30±0.70
NGC 4815	0.110±0.010	0.110±0.090	0.57±0.07	KIC 12069424	0.093±0.007	-0.090±0.009	7.00±0.50
NGC 6067	0.200±0.080	0.080±0.040	0.10±0.05	KIC 12069449	0.062±0.007	-0.085±0.009	7.10±0.50
NGC 6633	-0.010±0.110	0.080±0.020	0.52±0.10	KIC 12258514	0.027±0.007	-0.051±0.016	4.50±0.80
NGC 6802	0.100±0.020	0.170±0.020	1.00±0.10				
Pismis 18	0.220±0.040	0.050±0.040	1.20±0.04				
Trumpler 20	0.150±0.070	0.120±0.020	1.50±0.15				

References: * Casali et al. (2020) and references therein, † Nissen et al. (2017) and references therein

Delgado Mena et al. (2019) could determine the ages with a precision of 1.85 Gyr and MRE~57% using their 1D [Y/Mg] chemical clock. When using 2D relations, including $T_{eff}/[Fe/H]/mass$ as well, they got precisions and MRE (1.57 Gyr, 48%), (1.73 Gyr, 40%), and (1.71 Gyr, 37%), respectively, whereas their 3D relations (T_{eff} and [Fe/H] along with age) resulted in a precision of 1.47 Gyr with an MRE of 51%. The accuracy achieved by Titarenko et al. (2019) using their 1D dating relation is 2 Gyr. Meanwhile, the accuracy and precision of the chemical ages calculated using our relation (Eq. 5) are ~0.45 Gyr and 0.99 Gyr respectively, with a MRE of 33%. Since our sample lies in the solar neighbourhood, we have only discussed the results valid in this region.

5. Conclusions

Based on high-resolution and high-quality HARPS spectra, we have estimated the precise stellar atmospheric parameters and chemical abundances of Mg and Y through a line-by-line differential analysis for a sample of 48 metal-poor solar-type stars in the solar neighbourhood. Through the isochrone fitting method, stellar masses and ages of the sample were also estimated. We have performed a joint analysis of these 48 objects, together with 185 solar-twins and analogues from our previous studies. The combined sample consist of 233 solar-type stars in the solar neighbourhood, with metallicity in the range $-0.71 \leq [Fe/H] < +0.34$. The main results of our homogeneous analysis are summarised here.

- The sample shows a clear bimodality in the [Mg/Fe] - [Fe/H] plane, the thin and thick disk populations are clearly distinguishable. Thick disk stars show higher $[\alpha/Fe]$ values compared to thin disk stars. While the thick disk stars are older than 8 Gyr, the thin disk shows an age spread. Nonetheless, there is no age discontinuity between the two populations.
- Our chemically defined thick disk and thin disk stars show overlap in the kinematic space, a behaviour already noted in several previous studies.
- The thick disk stars show an Age-Metallicity-Relation, however, the age and metallicity exhibit an essentially flat distribution and are uncorrelated for the thin disk stars. On the other hand, both populations are blended in the Age - [Fe/H] distribution.

- There exists a correlation between [Mg/Fe] and stellar ages for both populations. However, in the case of [Y/Fe], only the thin disk stars show a correlation. We note a clear dichotomy between these two populations in the [Mg/Fe] - Age distribution, whereas there is no separation between them in the [Y/Fe] - Age space.
- The [Y/Mg] ratio shows strong anti-correlation with stellar age. Our analysis confirms the metallicity dependence of the [Y/Mg] chemical clock. We note the least scatter in the [Y/Mg] - Age distribution compared to previous studies of solar-type stars. There is no discontinuity between the thin and thick disks in the [Y/Mg] - Age correlation. Our estimates of the slope is compatible with those found for the solar-twins and other samples of solar-type stars in the higher metallicity bin ($[Fe/H] > -0.30$) as our sample.
- For the first time in the literature, we report similar slopes of [Y/Mg] - Age correlation for thin (-0.039) and thick disk (-0.034) stars.
- Using the dating relations (Eqs. 5 and 7), we could achieve high accuracies (0.67 and 0.45 Gyr, respectively) and precisions (0.96 and 0.99 Gyr, respectively). These accuracies are compatible with the best accuracy achieved for solar-twins till date (~0.8 - 1.0 Gyr) in the solar neighbourhood. The MRE in the chemical ages using these relations are 38% and 33%, respectively. The chemical clock based on the MV relation (Eq. 7) has somewhat better performance than the SV relations in two metallicity regimes (Eq. 5).

The relations connecting the abundance ratios and stellar ages are related to the chemo-dynamical evolution of the Galaxy, and can be used to study different components of it (Haywood et al. 2013, 2016). From our analysis, we found that the [Y/Mg] chemical clock can be used as an age proxy for the solar-type stars. The empirical relations showcased in this work should be used only for the stars in the solar neighbourhood, with the parameter range as our sample. The high-precision outcomes of our work are expected to provide contributions to the understanding of different populations of the Galaxy and its chemical evolution.

Acknowledgements. JS and JM acknowledge the support from FAPESP (2022/10325-3 and 2018/04055-8). This work made use of the SIMBAD astronomical database, operated at CDS, Strasbourg, France, and the NASA ADS, USA. This work has made use of data from the European Space Agency (ESA) mission *Gaia* (<https://www.cosmos.esa.int/gaia>),

Table 2: Slopes of [Y/Mg] - Age distribution of stars in the solar neighbourhood

Slope (dex Gyr ⁻¹)	N [†]	Pop [*]	Ref	Slope (dex Gyr ⁻¹)	N [†]	Pop [*]	[Fe/H]	Ref
solar-twins				solar-type				
-0.0404±0.0019	18	Thin disk	Nissen (2015)	-0.0362±0.0004	57		-0.71 - -0.17	This work
-0.0371±0.0013	21		Nissen (2016)	-0.0340±0.0006	166		-0.17 - +0.34	This work
-0.0410±0.0010	65		Tucci Maia et al. (2016)	-0.0390±0.0010	187	Thin disk	-0.71 - +0.34	This work
-0.0410±0.0017	45		Spina et al. (2016)	-0.0340±0.0010	36	Thick disk	-0.71 - +0.05	This work
-0.0460±0.0020	76		Spina et al. (2018)	-0.0347±0.0012	31		-0.15 - +0.15	Nissen et al. (2017)
-0.0420±0.0030	66	Thin disk	Spina et al. (2018)	-0.0199		Thin disk	-0.80 - -0.20	Delgado Mena et al. (2018)
-0.0410±0.0230		Thin disk	Delgado Mena et al. (2019)	-0.0420±0.0010	265	Thin disk	-0.60 - +0.55	Delgado Mena et al. (2019)
-0.0420±0.0030	80		Jofré et al. (2020)	-0.0290±0.0020	22	Thin disk	-0.80 - +0.40	Titarenko et al. (2019)
-0.0400±0.0020			Casali et al. (2020)	-0.0820±0.0020	11	Thick disk	-0.80 - +0.20	Titarenko et al. (2019)
				-0.0383±0.0010	68		-0.30 - +0.30	Nissen et al. (2020)
				-0.0270±0.0030	368	Thin disk	-0.60 - +0.40	Tautvaišienė et al. (2021) [‡]
				-0.0410±0.0130*	76	Thick disk	-0.46±0.12	Tautvaišienė et al. (2021)
				-0.0140±0.0040	66	Thick disk	-1.00 - +0.40	Tautvaišienė et al. (2021) (for Bensby et al. (2014) sample)
				-0.0020±0.0030	233	Thick disk	-1.00 - +0.40	Tautvaišienė et al. (2021) and references therein [‡]

[†] No. of stars used to derive the relation

* Fitting includes both the populations if not mentioned

[‡] Sample includes dwarf and giants

* Only giants

processed by the *Gaia* Data Processing and Analysis Consortium (DPAC, <https://www.cosmos.esa.int/web/gaia/dpac/consortium>). Funding for the DPAC has been provided by national institutions, in particular the institutions participating in the *Gaia* Multilateral Agreement. Based on data collected at the European Southern Observatory under ESO programs 60.A-9036(A), 60.A-9700(G), 60.A-9709(G), 072.C-0488(E), 073.C-0733(A), 077.C-0295(A), 077.C-0295(B), 078.C-0209(A), 080.C-0712(A), 082.C-0212(A), 082.C-0212(B), 084.C-0229(A), 085.C-0019(A), 085.C-0063(A), 086.C-0284(A), 087.C-0831(A), 088.C-0323(A), 089.C-0732(A), 091.C-0034(A), 091.C-0936(A), 092.C-0579(A), 092.C-0721(A), 093.C-0409(A), 094.C-0797(A), 096.C-0053(A), 096.C-0210(A), 098.C-0366(A), 106.21TJ.001, 183.C-0972(A), 184.C-0815(A), 184.C-0815(C), 184.C-0815(F), 190.C-0027(A), 192.C-0852(A), 196.C-0042, 196.C-0042(D), 196.C-0042(E), 0100.C-0097(A), 1102.C-0923(A), and 1102.C-0923(C).

References

- Adibekyan, V. Z., Figueira, P., Santos, N. C., et al. 2013, *A&A*, 554, A44
- Adibekyan, V. Z., Santos, N. C., Sousa, S. G., & Israelian, G. 2011, *A&A*, 535, L11
- Adibekyan, V. Z., Sousa, S. G., Santos, N. C., et al. 2012, *A&A*, 545, A32
- Alfredo Collazos, J. 2023, arXiv e-prints, arXiv:2308.08492
- Anders, F., Chiappini, C., Santiago, B. X., et al. 2014, *A&A*, 564, A115
- Babusiaux, C., Fabricius, C., Khanna, S., et al. 2022, arXiv e-prints, arXiv:2206.05989
- Bedell, M., Meléndez, J., Bean, J. L., et al. 2014, *ApJ*, 795, 23
- Bensby, T., Feltzing, S., & Lundström, I. 2003, *A&A*, 410, 527
- Bensby, T., Feltzing, S., Lundström, I., & Ilyin, I. 2005, *A&A*, 433, 185
- Bensby, T., Feltzing, S., & Oey, M. S. 2014, *A&A*, 562, A71
- Bergemann, M., Ruchti, G. R., Serenelli, A., et al. 2014, *A&A*, 565, A89
- Bland-Hawthorn, J. & Gerhard, O. 2016, *ARA&A*, 54, 529
- Bovy, J. 2015, *ApJS*, 216, 29
- Bovy, J., Rix, H.-W., & Hogg, D. W. 2012a, *ApJ*, 751, 131
- Bovy, J., Rix, H.-W., Liu, C., et al. 2012b, *ApJ*, 753, 148
- Cantelli, E. & Teixeira, R. 2024, *MNRAS*, 530, 2648
- Casagrande, L., Schönrich, R., Asplund, M., et al. 2011, *A&A*, 530, A138
- Casali, G., Magrini, L., Tognelli, E., et al. 2019, *A&A*, 629, A62
- Casali, G., Spina, L., Magrini, L., et al. 2020, *A&A*, 639, A127

- Casamiquela, L., Soubiran, C., Jofré, P., et al. 2021, *A&A*, 652, A25
- Castelli, F. & Kurucz, R. L. 2003, in Proceedings of the IAU Symp. No 210, Vol. 210, Modelling of Stellar Atmospheres, ed. N. Piskunov, W. W. Weiss, & D. F. Gray, A20
- Cayrel de Strobel, G. 1996, *A&A Rev.*, 7, 243
- Chaplin, W. J. & Miglio, A. 2013, *ARA&A*, 51, 353
- Christensen-Dalsgaard, J. 2016, arXiv e-prints, arXiv:1602.06838
- Cox, A. N. 2000, *Allen's astrophysical quantities* (Springer)
- da Silva, R., Porto de Mello, G. F., Milone, A. C., et al. 2012, *A&A*, 542, A84
- Delgado Mena, E., Moya, A., Adibekyan, V., et al. 2019, *A&A*, 624, A78
- Delgado Mena, E., Tsantaki, M., Zh. Adibekyan, V., et al. 2018, in *Astrometry and Astrophysics in the Gaia Sky*, ed. A. Recio-Blanco, P. de Laverny, A. G. A. Brown, & T. Prusti, Vol. 330, 156–159
- Edvardsson, B., Andersen, J., Gustafsson, B., et al. 1993, *A&A*, 275, 101
- Epstein, C. R., Johnson, J. A., Dong, S., et al. 2010, *ApJ*, 709, 447
- Feltzing, S., Holmberg, J., & Hurley, J. R. 2001, *A&A*, 377, 911
- Feltzing, S., Howes, L. M., McMillan, P. J., & Stokutė, E. 2017, *MNRAS*, 465, L109
- Fuhrmann, K. 1998, *A&A*, 338, 161
- Fuhrmann, K., Chini, R., Haas, M., et al. 2012, *ApJ*, 761, 159
- Gaia Collaboration, Prusti, T., de Bruijne, J. H. J., et al. 2016, *A&A*, 595, A1
- Gaia Collaboration, Vallenari, A., Brown, A. G. A., et al. 2022, arXiv e-prints, arXiv:2208.00211
- Gent, M. R., Eitner, P., Serenelli, A., et al. 2024, *A&A*, 683, A74
- Gilmore, G., Randich, S., Asplund, M., et al. 2012, *The Messenger*, 147, 25
- Haywood, M. 2006, *MNRAS*, 371, 1760
- Haywood, M. 2008, *A&A*, 482, 673
- Haywood, M., Di Matteo, P., Lehnert, M. D., Katz, D., & Gómez, A. 2013, *A&A*, 560, A109
- Haywood, M., Lehnert, M. D., Di Matteo, P., et al. 2016, *A&A*, 589, A66
- Howes, L. M., Lindegren, L., Feltzing, S., Church, R. P., & Bensby, T. 2019, *A&A*, 622, A27
- Imig, J., Price, C., Holtzman, J. A., et al. 2023, *ApJ*, 954, 124

- Jofré, P., Jackson, H., & Tucci Maia, M. 2020, *A&A*, 633, L9
- Karakas, A. I. & Lattanzio, J. C. 2014, *PASA*, 31, e030
- Kim, Y.-C., Demarque, P., Yi, S. K., & Alexander, D. R. 2002, *ApJS*, 143, 499
- Kobayashi, C., Umeda, H., Nomoto, K., Tominaga, N., & Ohkubo, T. 2006, *ApJ*, 653, 1145
- Lee, Y. S., Beers, T. C., An, D., et al. 2011, *ApJ*, 738, 187
- Leung, H. W., Bovy, J., Mackereth, J. T., & Miglio, A. 2023, *MNRAS*, 522, 4577
- Lin, J., Asplund, M., Ting, Y.-S., et al. 2020, *MNRAS*, 491, 2043
- Liu, C. & van de Ven, G. 2012, *MNRAS*, 425, 2144
- Martos, G., Meléndez, J., Rathsam, A., & Carvalho Silva, G. 2023, *MNRAS*, 522, 3217
- Matteucci, F. 2014, in *Saas-Fee Advanced Course, Vol. 37, Saas-Fee Advanced Course*, ed. J. Bland-Hawthorn, K. Freeman, & F. Matteucci, 145
- Meléndez, J., Bergemann, M., Cohen, J. G., et al. 2012, *A&A*, 543, A29
- Meléndez, J., Casagrande, L., Ramírez, I., Asplund, M., & Schuster, W. J. 2010, *A&A*, 515, L3
- Meléndez, J., Dodds-Eden, K., & Robles, J. A. 2006, *ApJ*, 641, L133
- Meléndez, J., Ramírez, I., Karakas, A. I., et al. 2014, *ApJ*, 791, 14
- Navarro, J. F., Abadi, M. G., Venn, K. A., Freeman, K. C., & Anguiano, B. 2011, *MNRAS*, 412, 1203
- Ness, M. K., Johnston, K. V., Blancato, K., et al. 2019, *ApJ*, 883, 177
- Nidever, D. L., Bovy, J., Bird, J. C., et al. 2014, *ApJ*, 796, 38
- Nissen, P. E. 2015, *A&A*, 579, A52
- Nissen, P. E. 2016, *A&A*, 593, A65
- Nissen, P. E., Christensen-Dalsgaard, J., Mosumgaard, J. R., et al. 2020, *A&A*, 640, A81
- Nissen, P. E., Silva Aguirre, V., Christensen-Dalsgaard, J., et al. 2017, *A&A*, 608, A112
- Nomoto, K., Kobayashi, C., & Tominaga, N. 2013, *ARA&A*, 51, 457
- Patil, A. A., Bovy, J., Jaimungal, S., Frankel, N., & Leung, H. W. 2023, *MNRAS*, 526, 1997
- Ramírez, I. & Meléndez, J. 2005, *ApJ*, 626, 446
- Ramírez, I., Meléndez, J., & Asplund, M. 2009, *A&A*, 508, L17
- Ramírez, I., Meléndez, J., Bean, J., et al. 2014, *A&A*, 572, A48
- Randich, S., Gilmore, G., & Gaia-ESO Consortium. 2013, *The Messenger*, 154, 47
- Rathsam, A., Meléndez, J., & Carvalho Silva, G. 2023, *MNRAS*, 525, 4642
- Reddy, B. E., Lambert, D. L., & Allende Prieto, C. 2006, *MNRAS*, 367, 1329
- Rix, H.-W. & Bovy, J. 2013, *A&A Rev.*, 21, 61
- Sahlholdt, C. L., Feltzing, S., & Feuillet, D. K. 2022, *MNRAS*, 510, 4669
- Salaris, M., Chieffi, A., & Straniero, O. 1993, *ApJ*, 414, 580
- Schirbel, L., Meléndez, J., Karakas, A. I., et al. 2015, *A&A*, 584, A116
- Schönrich, R. & Binney, J. 2009, *MNRAS*, 396, 203
- Schönrich, R., Binney, J., & Dehnen, W. 2010, *MNRAS*, 403, 1829
- Schuster, W. J., Moitinho, A., Márquez, A., Parrao, L., & Covarrubias, E. 2006, *A&A*, 445, 939
- Shejeelammal, J. & Goswami, A. 2024, *MNRAS*, 527, 2323
- Silva Aguirre, V., Casagrande, L., Basu, S., et al. 2012, *ApJ*, 757, 99
- Silva Aguirre, V., Lund, M. N., Antia, H. M., et al. 2017, *ApJ*, 835, 173
- Skúladóttir, Á., Hansen, C. J., Salvadori, S., & Choplin, A. 2019, *A&A*, 631, A171
- Slumstrup, D., Grundahl, F., Brogaard, K., et al. 2017, *A&A*, 604, L8
- Snedden, C., Bean, J., Ivans, I., Lucatello, S., & Sobeck, J. 2012, *MOOG: LTE line analysis and spectrum synthesis*, Astrophysics Source Code Library, record ascl:1202.009
- Snedden, C. A. 1973, PhD thesis, THE UNIVERSITY OF TEXAS AT AUSTIN.
- Soderblom, D. R. 2010, *ARA&A*, 48, 581
- Soderblom, D. R. & King, J. R. 1998, in *Solar Analogs: Characteristics and Optimum Candidates.*, ed. J. C. Hall, 41
- Spina, L., Meléndez, J., Karakas, A. I., et al. 2018, *MNRAS*, 474, 2580
- Spina, L., Meléndez, J., Karakas, A. I., et al. 2016, *A&A*, 593, A125
- Tautvaišienė, G., Viscasillas Vázquez, C., Mikolaitis, Š., et al. 2021, *A&A*, 649, A126
- Titarenko, A., Recio-Blanco, A., de Laverny, P., Hayden, M., & Guiglion, G. 2019, *A&A*, 622, A59
- Tucci Maia, M., Ramírez, I., Meléndez, J., et al. 2016, *A&A*, 590, A32
- Viscasillas Vázquez, C., Magrini, L., Casali, G., et al. 2022, *A&A*, 660, A135
- Weinberg, D. H., Holtzman, J. A., Hesselquist, S., et al. 2019, *ApJ*, 874, 102
- Xiang, M. & Rix, H.-W. 2022, *Nature*, 603, 599
- Yana Galarza, J., Meléndez, J., Ramírez, I., et al. 2016, *A&A*, 589, A17
- Yanny, B., Rockosi, C., Newberg, H. J., et al. 2009, *AJ*, 137, 4377
- Yi, S., Demarque, P., Kim, Y.-C., et al. 2001, *ApJS*, 136, 417

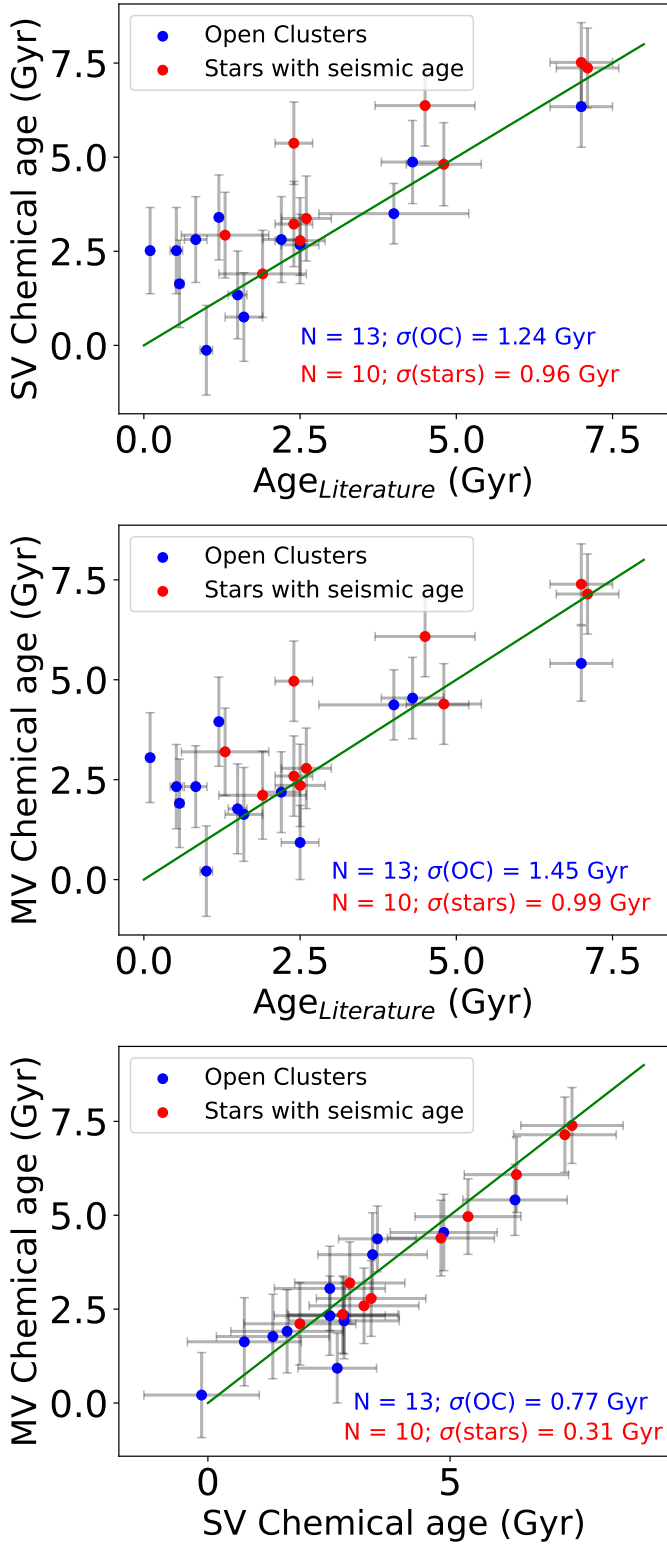


Fig. 10: Comparison of the literature ages of the OCs and KLS stars with their single variate (SV; upper panel) and multivariate (MV; middle panel) chemical ages. The bottom panel shows the correlation between the two chemical ages. The green line represents the one-to-one fit.

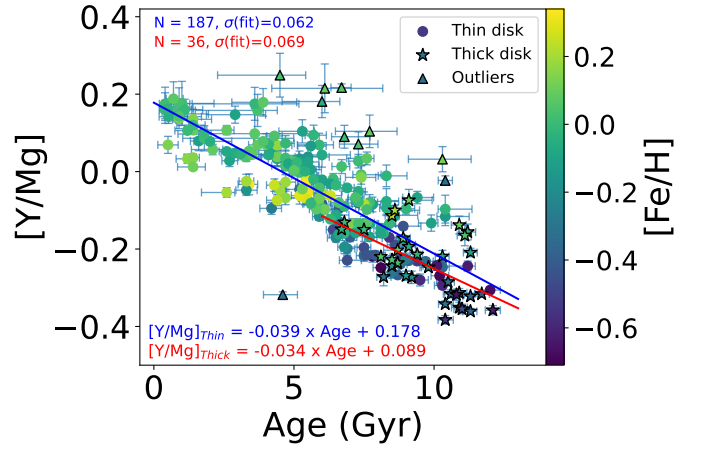


Fig. 11: Best linear fits for thin (blue solid line) and thick disk (red solid line) stars separately. The fitting functions are described in the text.

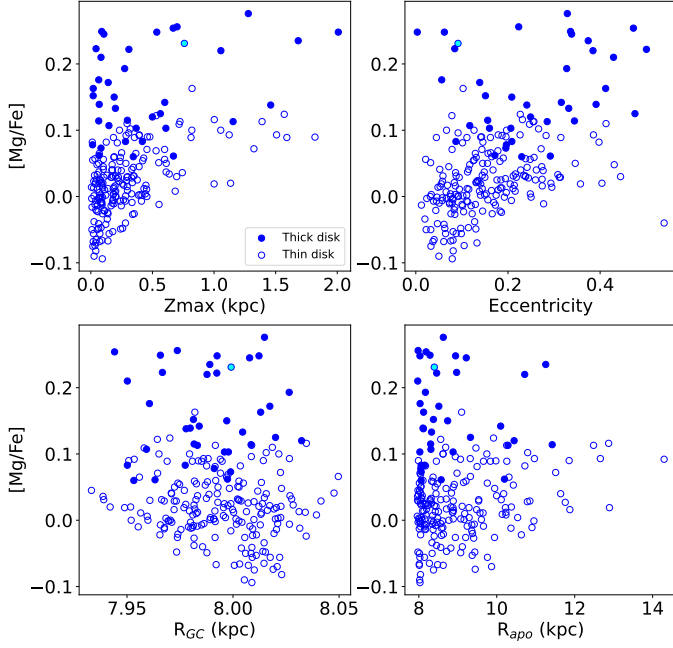


Fig. B.1: Observed $[Mg/Fe]$ of the entire sample with respect to various orbital parameters. The cyan circle is the anomalous star HD 65907.

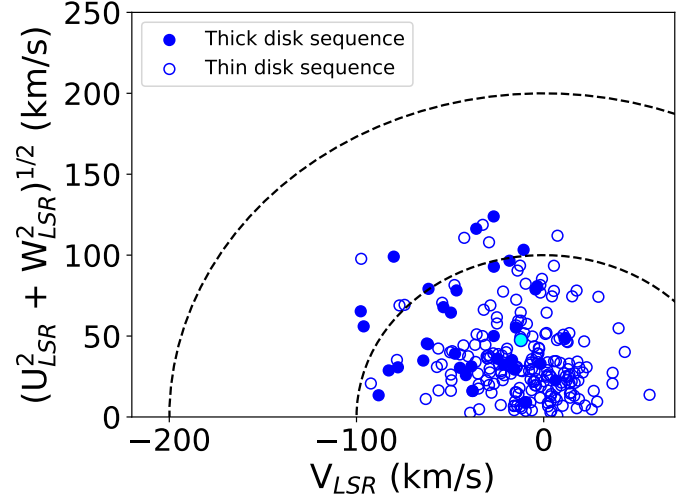


Fig. B.2: Toomre diagram for the entire sample. The dotted inner and outer circles have radii 100 km/s and 200 km/s, respectively.

Appendix B: Kinematics of the stellar sample

Various orbital characteristics and Galactic space velocities of the sample are calculated using the `galpy` (<http://github.com/jobovy/galpy>) Python package (Bovy 2015). The components of spatial velocities (U , V , and W) are calculated with respect to the Local Standard of Rest (LSR) and the adopted solar motion about the LSR is $(U, V, W)_\odot = (11.1, 12.2, 7.3)$ km/s (Schönrich et al. 2010). The detailed procedure can be found in Shejeelammal & Goswami (2024). The behaviour of the $[Mg/Fe]$ ratio observed in the sample as functions of maximum height above the Galactic plane (Z_{max}), eccentricity, Galactocentric distance (R_{GC}) and apocentric distance (R_{apo}) are shown in Fig. B.1. The Toomre diagram for the sample is shown in Fig. B.2. As can be seen, it is difficult to separate the thin and thick disk from purely kinematic criteria.